Total Synthesis Hot Paper

How to cite: *Angew. Chem. Int. Ed.* **2022,** *61,* e202209105
International Edition: doi.org/10.1002/anie.202209105
German Edition: doi.org/10.1002/ange.202209105

Total Synthesis and Functional Evaluation of IORs, Sulfonolipid-based Inhibitors of Cell Differentiation in *Salpingoeca rosetta*

*Luka Raguž[+], Chia-Chi Peng[+], Florentine U. N. Rutaganira, Thomas Krüger, Aleksa Stanišić, Theresa Jautzus, Hajo Kries, Olaf Kniemeyer, Axel A. Brakhage, Nicole King, and Christine Beemelmanns**

Dedicated to Professor Jon Clardy on the occasion of his birthday

Abstract: The choanoflagellate *Salpingoeca rosetta* is an important model system to study the evolution of multicellularity. In this study we developed a new, modular, and scalable synthesis of sulfonolipid IOR-1A (six steps, 27 % overall yield), which acts as bacterial inhibitor of rosette formation in *S. rosetta.* The synthesis features a decarboxylative cross-coupling reaction of a sulfonic acid-containing tartaric acid derivative with alkyl zinc reagents. Synthesis of 15 modified IOR-1A derivatives, including fluorescent and photoaffinity-based probes, allowed quantification of IOR-1A, localization studies within *S. rosetta* cells, and evaluation of structure-activity relations. In a proof of concept study, an inhibitory bifunctional probe was employed in proteomic profiling studies, which allowed to deduce binding partners in bacteria and *S. rosetta.* These results showcase the power of synthetic chemistry to decipher the biochemical basis of cell differentiation processes within *S. rosetta.*

[*] L. Raguž,[+] C.-C. Peng,[+] Dr. T. Jautzus, Prof. C. Beemelmanns
Chemical Biology of Microbe-Host Interactions, Leibniz Institute for Natural Product Research and Infection Biology, Hans-Knöll-Institute (HKI),
Beutenbergstraße 11a, 07745 Jena (Germany)
E-mail: Christine.Beemelmanns@leibniz-hki.de

Dr. F. U. N. Rutaganira, Prof. N. King
Life Sciences Addition,
University of California, Berkeley
Berkeley, CA 94720 (USA)

Dr. T. Krüger, Dr. O. Kniemeyer, Prof. A. A. Brakhage
Molecular and Applied Microbiology, Leibniz Institute for Natural Product Research and Infection Biology, Hans-Knöll-Institute (HKI)
Beutenbergstraße 11a, 07745 Jena (Germany)

A. Stanišić, Dr. H. Kries
Biosynthetic Design of Natural Products, Leibniz Institute for Natural Product Research and Infection Biology, Hans-Knöll-Institute (HKI)
Beutenbergstraße 11a, 07745 Jena (Germany)

Prof. A. A. Brakhage
Microbiology and Molecular Biology,
Institute of Microbiology, Friedrich Schiller University (FSU)
Neugasse 25, 07743 Jena (Germany)

Prof. C. Beemelmanns
Biochemistry of Microbial Metabolism,
Institute of Biochemistry, Leipzig University
Johannisallee 21–23, 04103 Leipzig (Germany)

[+] These authors contributed equally to this work.

Introduction

Choanoflagellates are water-dwelling predators of bacteria and have emerged as an important model system to study the evolution of multicellularity due to their phylogenetic placement as the closest living single-celled relatives of animals.[1,2] While predominately unicellular, several choanoflagellate species have multicellular life stages, including rosette colonies that arise from serial cell division without separation of sister cells. Rosettes are presumed to have a fitness advantage over single cells as increased water fluxes around rosettes allow predation on more bacterial cells per unit time.[3]

In the choanoflagellate *Salpingoeca rosetta*, multicellular rosette development is induced after sensing of bacterial signaling biomolecules (Figure 1).[4,5] One rosette-inducing bacterium, *Algoriphagus machipongonensis* PR1, produces a plethora of sulfonosphingolipids as a major constituent of the bacterial cell membrane,[6,7] two of which have rosette-inducing activity (RIF-1 and RIF-2)[8,9] while RIF-homologs sulfobacin D, F and sulfonolipid IOR-1A both antagonize the rosette inducing capacity in a dose-dependent fashion.[10]

Intriguingly, the effect of both RIF molecules, and mixtures thereof, are synergistically enhanced in the presence of two co-occurring lysophosphatidylethanolamine derivatives (LPEs) derived from the same bacterium.[11–13] The unique phylogenetic placement of choanoflagellates and the ecological relevance of the choanoflagellate-bacteria symbiosis prompted us to investigate the role and fate of bacterial sulfonolipids within this peculiar cross-kingdom interaction.[14,15]

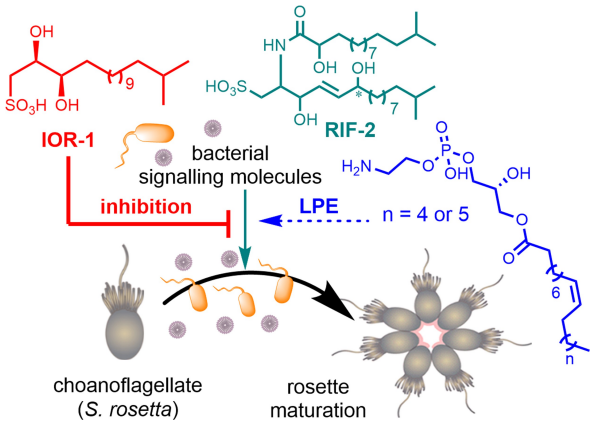

Figure 1. Bacterial sulfonosphingolipids mediate predator-prey interaction between *S. rosetta* and *A. machipongonensis*.

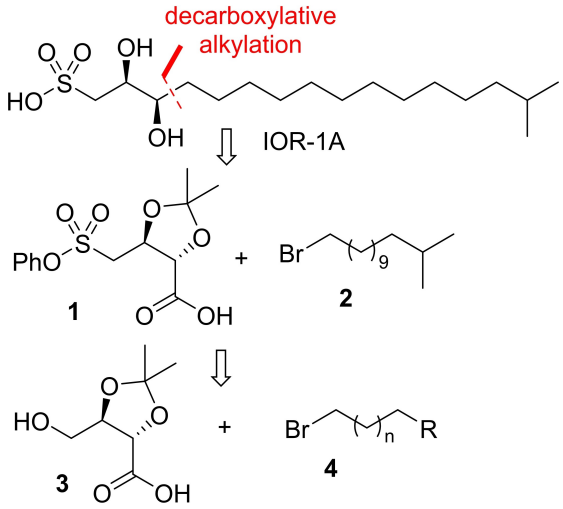

Scheme 1. Retrosynthesis of IOR-1A based on a Ni-catalyzed decarboxylative cross-coupling reaction sequence.

In this study, we investigated the hypothesis that sulfonolipids are not only integral parts of bacterial membranes,[16,17] but also interact with dedicated sphingolipid binding partners in the producing organism *A. machipongonensis* and the recipient *S. rosetta*.[18] To profile potential cellular binding partners, we developed an efficient synthesis of photo-reactive sulfonolipid probes structurally resembling inhibitor IOR-1A using a combination of decarboxylative cross-coupling reaction and late-stage functionalization reactions.[19–21] Bioassay studies confirmed that our designed probes retained inhibitory activity of rosette formation with a clear structure-activity relation (SAR). The fluorescence-based IOR-1A probes allowed us to track their incorporation into what appeared to be food vacuoles in *S. rosetta* and photoaffinity probes enabled the first proteome-wide unbiased target profiling. Results of this proof of concept study enabled the de novo identification of noncovalent protein binders of IOR-1A in bacteria and *S. rosetta*, and thus improve our understanding of sulfonolipids as cellular and cross-kingdom communication signal of pre-metazoan origin.

Results and Discussion

Total Synthesis of IOR-1A and Congeners

In our retrosynthetic considerations of IOR-1A, we envisaged the usage of chiral pool reagents with pre-defined stereochemistry and a modular cross-coupling reaction sequence that would allow the incorporation of various chain derivatives without loss of stereochemical information (Scheme 1). Based on our[22] and other reports,[23–26] a decarboxylative alkylation approach using a desymmetrized tartaric acid derivative **1** and alkyl zinc reagent, derived from alkyl bromide **2**, appeared to be most suited to enable a quick and modular approach towards IOR-1A.

Thus, our synthesis commenced with literature known tartaric acid derivate **3**,[27] which was synthesized from D-tartaric acid in two steps.[28] Subsequent substitution of the hydroxyl group under Mitsunobu conditions afforded thioacetate **5** in excellent yield (Scheme 2A), which was followed by oxidation of the sulfur to the intermediate sulfonyl chloride **6** and direct conversion to sulfonoester **7** by addition of different alcohols.[29]

Sulfonoesters were then evaluated for their stability towards saponification and Ni-catalyzed decarboxylative cross coupling conditions. Literature studies indicated that in particular trichloroethyl sulfonic esters (**7a**) were reported to withstand harsh acidic reaction conditions,[29] while isobutyl (**7b**) and neopentyl sulfonic esters (**7c**) were stable towards bases and nucleophiles and were cleaved after treatment with strong acids.[30] Subsequent screening of reaction conditions uncovered that only isobutyl (**7b**), neopentyl (**7c**) and phenyl (**7e**) sulfonic esters were suitable protecting groups (Table S1). Due to its balanced stability profile towards mild basic conditions, the best overall yields were obtained with phenyl sulfonate **7e** affording carboxylic acid **8** in 91 % on a multi-gram scale (Scheme 2B).[30]

We then turned our attention towards optimizing the reaction conditions for the envisaged decarboxylative cross-coupling reaction of **8** and **10**. First, an extensive screening of nickel salts and ligands was pursued to optimize yield and selectivity of the cross-coupling reaction of **8** and dihexyl zinc as test reagent (prepared by transmetalation of commercially available hexylmagnesium bromide, Table S2). Overall, the combination of activation reagent CITU (1,1,3,3-tetramethyl-2-(4,5,6,7-tetrachloro-1,3-dioxoisoindolin-2-yl)isouronium hexafluoro-phosphate(V)),[23,26] $NiCl_2$·glyme, bipyridine and dihexyl zinc afforded compound **9b** in 59 % yield and under retention of stereochemistry (*dr* 14:1, Table S3 and S4).[22]

Encouraged by these promising results, we then investigated the applicability of different alkyl zinc reagents (**10**) in the decarboxylative alkylation reaction and were pleased to find that different chain length derivatives (**9a–d**) and functionalized side chains (**9e–f**) underwent cross-coupling reactions in moderate to good yields. The high diastereose-

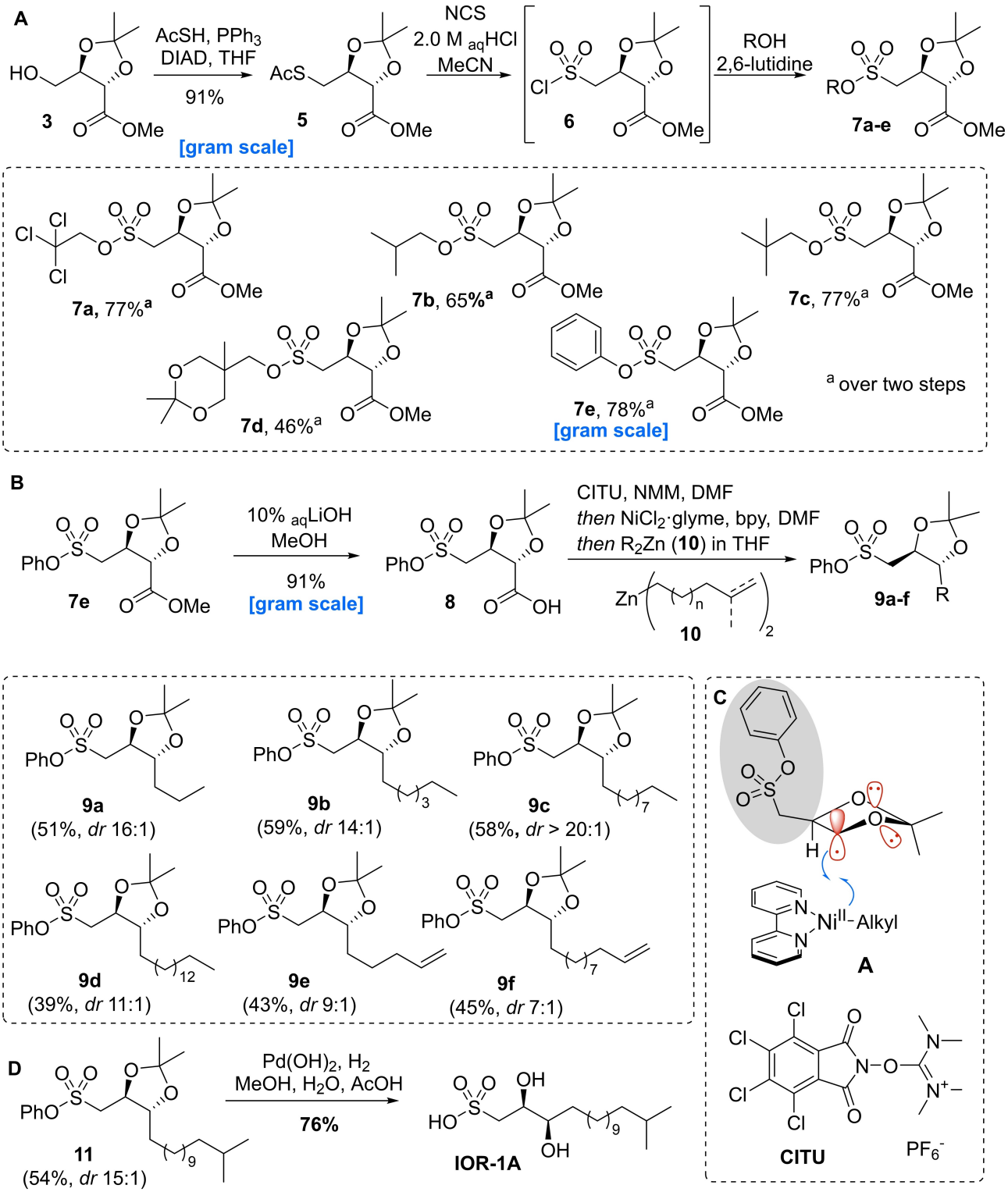

Scheme 2. A) Synthesis of protected sulfonic esters using a three-step procedure; B) Decarboxylative alkylation reaction of tartaric acid derivative **8** and different alkyl zinc reagents [R_2Zn (**10**)] with resulting products **9** and **11**; C) Proposed intermediate A of the cross-coupling step initiated by the activation reagent CITU; D) Reductive removal of protecting groups results in the formation of IOR-1A.

lectivity of the coupling reaction most likely originates from the interaction of the SUMO with the neighboring oxygen lone pair orbital (red) which stabilizes the ring conformation of radical **A** and sterical interactions (grey), which allows the approach of the catalyst complex predominantly from the opposite side (Scheme 2C).[31–33]

In proof-of-concept studies, the deprotection sequence was optimized using compound **9b** as model substrate. First,

acidic deprotection conditions were employed to release the protected diol, followed by hydrolyzation of the sulfonate ester (Table S5 and S6); however, due to the intrinsic reactivity of the resulting products, the formation of various side products was observed.

While a change of the deprotection sequence (first saponification, then release of diol) did not provide the desired IOR-1A derivative, acidic hydrogenation conditions using Pearlman's catalyst and H_2 finally resulted in the global deprotection of **9b**.[34] Selective deprotection of only the sulfonate ester was achieved when zinc dust was employed to generate H_2 *in situ.* Encouraged by these results, we finalized the synthesis of IOR-1A in overall six steps from **3** and 27 % total yield and were delighted to find that all analytical data of synthesized IOR-1A agreed with previously published literature data (Scheme 2D, Table S7).[10] With this modular synthesis in hand, we then focused on the synthesis of IOR1-A derivatives that could be easily transformed to bifunctional chemical probes carrying either fluorophores or groups suitable for photoaffinity labeling.[19–21] As the final global deprotection step of the synthesis included acidic and reductive reaction conditions, introduction of functional groups was required prior to the deprotection step. As depicted in Scheme 3A, terminal alkene derivatives **9e** and **9f** were easily converted under hydroboration/oxidation conditions to the primary alcohols **12a** and **12b**,[35] and under hydroamination conditions[36] to primary amines **13a** and **13b**. Sulfonic esters were deprotected under reductive conditions affording the corresponding sulfonic acids **14a**–**14g** in up to 89 % yield (Scheme 3B, green). Due to the cellular stability of amides compared to e.g. esters, deprotected amine sulfonic acids **14f** and **14g** were further converted to different mono and bifunctional probes (**15**–**18**, blue) in good yields using peptide coupling conditions. To our delight, optimized reaction conditions required only one final purification step in the two-step procedure.

IOR-1A Congeners Exhibit Structure-related Inhibitory Activity

Next, we evaluated the effect of IOR-1A on growth and the inhibitory effect of IOR-1A derivatives on rosette formation of *S. rosetta.*[10] Dose-response assays showed that *A. machipongonensis* PR1 and *Echinicola pacifica* KMM 6172 tolerated IOR-1A concentrations of up to 5 μM without any visible morphological changes (Figure S1), while *S. rosetta* cell lines started to show signs of impaired cell swimming behavior and reduced proliferation above 2 μM.

To test rosette-inhibition activity, single celled *S. rosetta* cultures were incubated with constant concentrations of RIF-2 to induce rosette formation and varying, but non-toxic concentrations of IOR-1A derivatives (Figure S1). To our delight, several chain length derivatives (**14a**–**14d**, Scheme 3C) caused the inhibition of rosette formation in up to 80 % of all cells relative to IOR-1A . These results suggested that structural changes related to chain length and branching pattern influenced the activity only moderately, while changes in stereochemistry abolished bioactivities.[10] Surprisingly, the presence of an amide group in proximity to the polar head (**15a**) caused an activity loss whereas derivatives carrying longer amide linkages (**15b**) exhibited about 70 % of IOR-1A's inhibition strength. Slightly decreased inhibition activity was also observed when other functional groups with similar chain length were introduced. Importantly, bifunctional probes inhibited rosette formation, of which nitrobenzoxadiazole (NBD) and benzophenone derivatives (**16** and **18**) exhibited the best inhibitory activities (70–80 % compared to IOR-1A) making them viable tools for the identification of IOR-1A targets.

IOR-1A Is a Component of the Bacterial Cell Membrane

The availability of synthetic IOR-1A and congeners allowed us to solve our long-standing question in which quantities IOR-1A and congeners are produced by sulfonosphingolipid-producing bacterial strains, such as rosette-inducing members of the genus *Algoriphagus*, *Cyclobacterium marinum* LMG 13164, *Belliella baltica* BA134, *Dyadobacter fermentans* DSM 18053, *Zobellia uliginosa* ATCC 14397, and the non-inducing co-occurring bacterial prey bacterium *E. pacifica* KMM 6172 (Figure 2).[4]

Using an LC-MS/MS based approach, we confirmed that six members of the genus *Algoriphagus* as well as the strains *C. marinum* and *D. fermentans* produced IOR-1A in similar amounts (based on biomass obtained from a 10 mL culture with $OD_{600} = 0.8$, Table S8, Figure S2). In contrast, only negligible concentrations were detectable in *B. baltica*, *Z. uliginosa* and the non-inducing co-cultured strain *E. pacifica.* Notably, growth conditions and age had a strong influence on the detectable concentration of IOR-1A in all producing strains as growth in marine broth, for instance, resulted in about 5-fold more IOR-1A compared to growth in sea water complete medium (SWC).

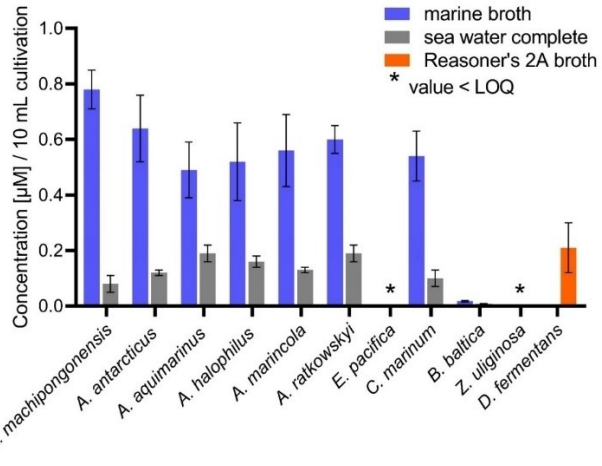

Figure 2. LC–MS/MS-based analysis: quantification of IOR-1A (m/z 351.22 $[M-H]^-$) in bacterial cell pellets of *A. machipongonensis* PR1, *A. antarcticus* LMG 21980, *A. aquimarinus* LMG 21971, *A. halophilus* DSM 15292, *A. marincola* SW-2, *A. ratkowskyi* LMG 21435 grown under three different growth conditions ($n = 3$) (LOQ: limit of quantification).

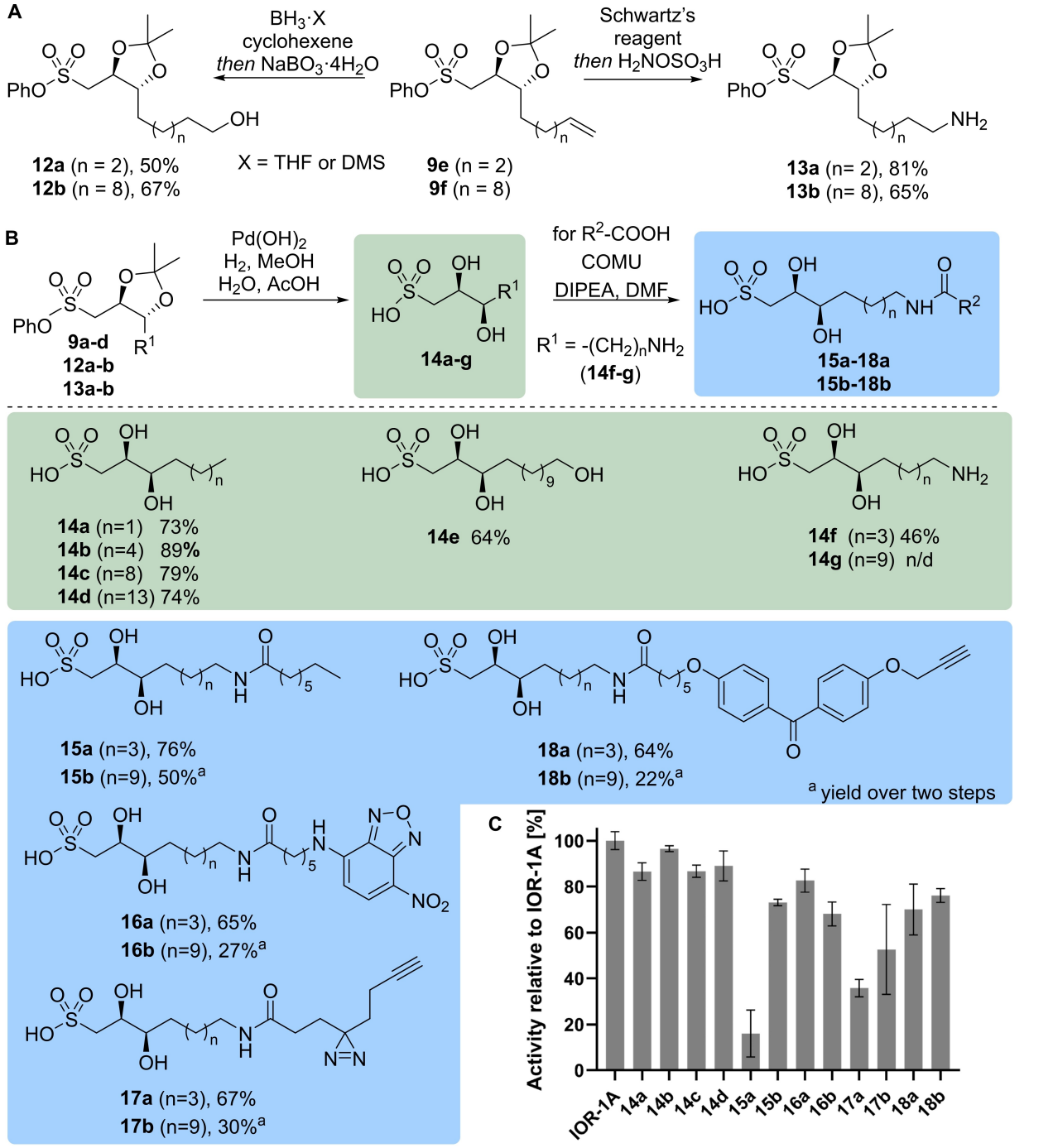

Scheme 3. Synthesis of mono- and bifunctionalized IOR-1A derivatives; A) Introduction of heteroatoms at the late stage using two different synthetic strategies; B) Deprotection and amidation sequence leading to sixteen IOR-1A derivatives carrying different functionalities; C) Inhibition of rosette formation in *S. rosetta* by IOR-1A derivatives relative to IOR-1A in the presence of rosette-inducing RIF-2 (30 μM) ($n = 3$, error bars showing standard deviation generated by GraphPad Prism 9 statistical software).

To test if IOR-1A is enriched within one of the bacterial cell membranes, we analyzed enriched inner and outer membrane layers of our model strain *A. machipongonensis* PR1 separately.[37] Here, we found that outer membrane fractions contained higher abundances compared to inner membrane fractions or mixtures of both (Table S10). We also analyzed isolated outer membrane vesicles (OMV) that are naturally shed from *A. machipongonensis* PR1 into the culture supernatant and which were obtained from the same 10 mL culture; however, due to the naturally low biomass of OMVs, only negligible concentrations of IOR-1A were detectable.

Sulfonosphingolipids and LPEs Localize within Vacuoles

S. rosetta cells are filter feeding heterotrophic nanoflagellates and prey on bacterial cells, which are phagocytosed and digested in anterior localized food vacuoles.[38–40] Thus, membrane components, including sulfonolipids with signalling functions (e.g. IOR-1A, RIFs, or synergizing LPEs) likely accumulate within these food vacuoles, from where they might start interfering with cellular processes. To test this hypothesis, we first exposed healthy *S. rosetta* cells to nitrobenzoxadiazole (NBD)-labeled (lyso)phospholipid, NBD-18:1 LPE (5 μM) and phospholipid NBD-18:1–12:0 PE (5–25 μM). As depicted in Figure 3a and b, phospholipids accumulated within hours in intracellular vesicles, which appeared to be intracellular food vacuoles,[39,40] while no accumulation of 6-(7-nitrobenzofurazan-4-ylamino)-hexanoic acid was observed (Figure S5, S6). Intriguingly, treatment with 18:1 NBD LPE caused a strong fluorescence signal at a concentration of 5 μM, while treatment with 18:1–12:0 NBD PE required higher concentrations (25 μM) to cause fluorescence signals of similar intensities. Although biochemical reasons for the observed substrate specificity remain unclear, the result clearly demonstrated the uptake of phospholipids.

Subsequently, *S. rosetta* cells were incubated with either LysoTracker Blue DND-22 (1 μM) to stain acidic compartments in live cells or probes **16a** and **16b** (5 μM) to monitor the fate of IOR-derivatives within living cells (Figure 3c–e, Figure S5, S6). After one-hour of incubation, IOR-1A derivative **16b** as well as LysoTracker Blue DND-22 were clearly detectable within the same intracellular location of healthy cells. Analogously to prior studies with phospholipids, the intensity of accumulation within vacuoles was dependent on the structure as the fluorescence signals of shorter chain-length derivative **16a** was less intense compared to derivative **16b** with similar chain-length as IOR-1A.

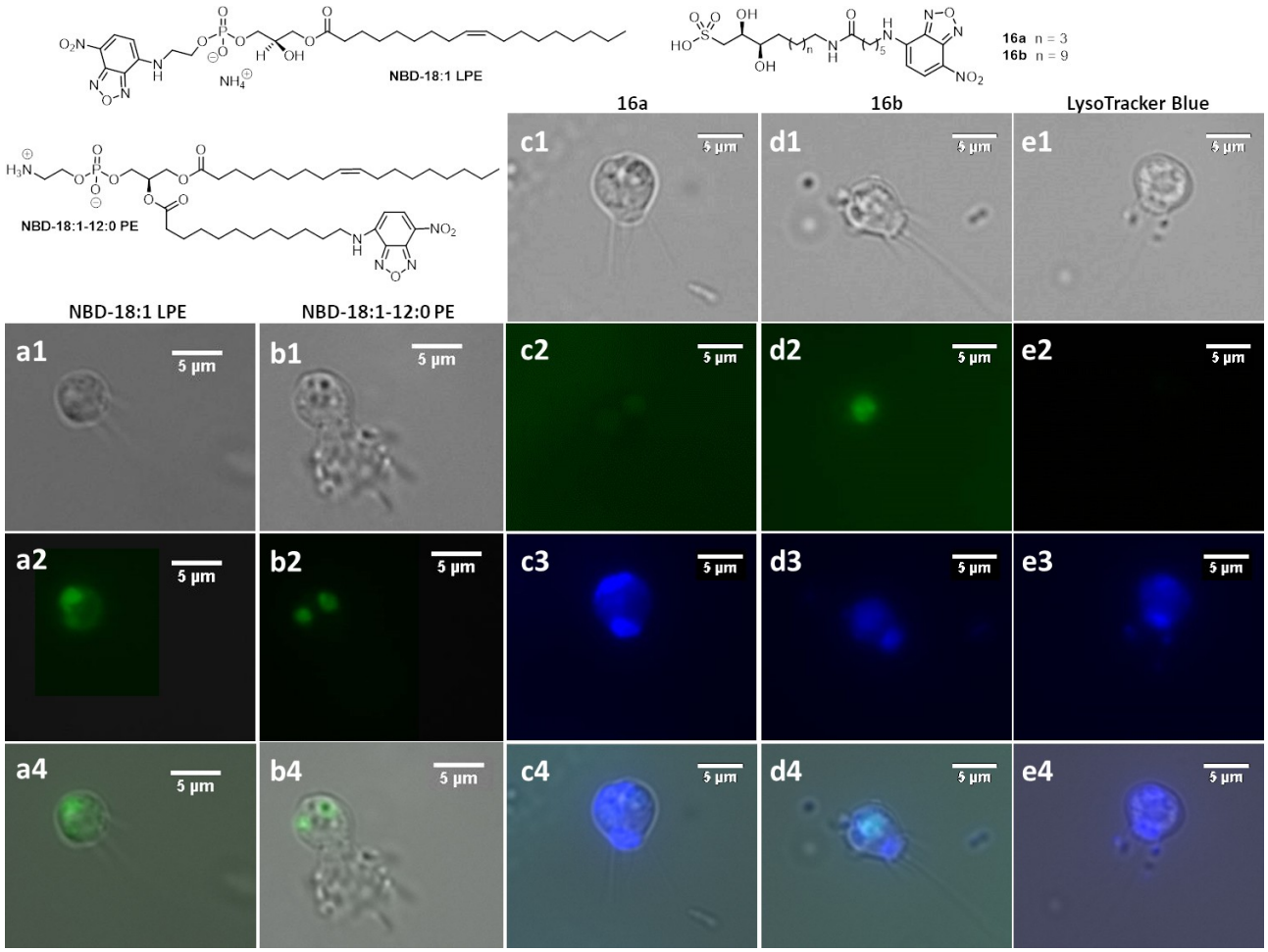

Figure 3. Structures of NBD labelled probes and microscopy images of *S. rosetta* cells in which NBD labelled probes accumulate in food vacuoles 4–5 h after treatment ($n=3$) with a) 5 μM NBD-18:1 LPE; b) 25 μM NBD-18:1–12:0 PE; c) 5 μM **16a**/1 μM LysoTracker Blue DND-22; d) 5 μM **16b**/1 μM LysoTracker Blue DND-22; e) 1 μM LysoTracker Blue DND-22 with (1) bright-field; (2) emission wavelength of 535 nm (NBD); (3) Emission wavelength of 422 nm (LysoTracker Blue DND-22); (4) Overlaid pictures (DMSO served as negative control, Figure S5, S6).

Chemical Probes of IOR-1A Are Suitable for Proteomic Profiling

Inspired by the localization of IOR-1A probes in *S. rosetta* and its structural resemblance to the sphingolipid precursor 3-ketodihydrosphingosine (3-KDS),[12,13] and other signaling molecules such as sphingosine-1-phosphate (S1P) or the ceramide synthase inhibitor fumonisin,[41] we questioned if IOR-1A interacts with enzymes involved in the sphingolipid metabolism in both bacteria and *S. rosetta.* While the enzymology of bacterial (sulfono)sphingolipid biosynthesis including *A. machipongonensis* has recently gained much attention in the literature (Figure S13),[42,43] sphingolipid metabolism in *S. rosetta* has not yet been explored. Thus, we performed a BLAST search of the annotated genome of *S. rosetta* and indeed identified several protein homologs of known eukaryotic sphingolipid-related biosynthetic enzymes (Table S11). These findings indicated that *S. rosetta* might employ sphingolipid signaling mechanisms to orchestrate cellular mechanisms and its life style, and which could interact with phagocytosed bacterial sulfonolipids.

To profile dedicated binding partners in either bacteria or *S. rosetta*, a label-free quantification (LFQ) protocol using compounds **18a–b** was pursued as these probes fulfilled four key requirements:[44,45] (1) Mimic parent compound IOR-1A, (2) retain inhibitory activity, (3) contain photo-activatable chemical functionality that upon *in situ* sample irradiation covalently cross-link to a molecule/protein in close proximity, and (4) carry a biorthogonal handle for selective pull-down of the probe-protein complex from cell lysate.

After intensive studies of possible photo-cross-coupling conditions using **18a** and **18b**,[20,46,47] IOR-derivative **18a** and two sample types [intact cells (sample A) and enriched proteins of lysed cells (sample B)] were selected for further studies. In short, the following photo-affinity strategy was employed: biosamples ($n=3$) were treated with **18a** (2 h) and either subjected to photo-cross-linking conditions (+UV) or kept in the dark (non-irradiated control samples (−UV)). Coupling was performed with 5/6-TAMRA-Azide-Biotin, which yielded, after enrichment with streptavidin-covered magnetic beads, the biotinylated protein samples (Figure 4A). Sodium dodecyl sulfate polyacrylamide gel electrophoresis (SDS-PAGE) confirmed successful cross-linking by comparing protein fingerprints of UV-irradiated samples and non-irradiated controls by in-gel fluorescence (Figure 4A, Figure S5, S6). Peptide fragments of samples obtained from enzymatic digests of proteins on-beads and excised gel bands (in-gel) were analyzed by nano-liquid chromatography tandem mass spectrometry (nano-LC-ESI MS/MS) (Figure S6, Table S12–S24, and data deposited to the ProteomeXchange Consortium via the PRIDE partner repository with the dataset identifier PXD034064).[48] Analysis of datasets derived from *A. machipongonensis, E. pacifica, and S. rosetta* biosamples showed that the most peptide sequences were identified from *A. machipongonensis* samples [1889 (cell lysates); 1509 (intact cells) with 1341 shared features], while samples from *E. pacifica* [(467 (intact cells), 51 (cell lysate) with 28 shared features] and S. rosetta-*E. pacifica* cell lines [(total of 210 *E. pacifica*-specific, 42 *S. rosetta*-specific candidate sequences] resulted repeatedly in fewer candidate sequences (Figure 4C, D and S7, S8).

IOR-1A Interacts with Metabolic Enzymes of Bacterial Origin

We used manually curated gene ontology-(GO)-assisted analysis (Figure S9–S11) to associate significant bacterial protein hits (threshold of $\log_2(+\text{UV}/-\text{UV}) > 6$ with a p-value < 0.0001; Figure 4B–D) with predicted cellular function and localization.[49] The most significant protein hits in all four bacterial samples were assigned to membrane-bound ATP-binding transporters, redox-active fatty acid synthesis (FAS)-related enzymes,[50] amino acid-related transferases, kinases, and other modifying enzymes, as well as peptide- and sulfur metabolism-related hydrolases. Several protein hits related to enzymes involved in the sulfonosphingolipid biosynthesis and degradation pathways were detectable in most bacterial datasets (Table S11),[42,43,51,52] which led us to hypothesize that IOR-1A could be biosynthetically derived from a sulfono-3-ketodihydro-sphingosine (3-KDS) derivative, via a transamination step and reduction at C-2, presumably catalyzed by a ceramide reductase (CerR) or a NADPH-dependent 3-ketodihydro-sphingosine reductase (KDSR, EC 1.1.1.102) (Figure S13). Furthermore, a homolog of the ceramide synthase (CerS) was identified as a significant binding partner, which allows to speculate if IOR-1A might serve as inhibitory modulator of CerS, similar to the function of fumonisins.[41]

Although with low significance, it was also intriguing to note that not only a homolog of the chondroitinase EroS, which induces mating in *S. rosetta*,[53] but also a homolog of the gliding motility-associated lipoprotein (GldJ)[54,55] was listed as possible binding partner. Overall, the multitude of identified putative bacterial binding partners involved in sphingolipid biosynthesis, metabolism and physiology strongly support the hypothesis that IOR-1A holds not only structural functions, but also signaling and even regulatory functions.

IOR-1A Interacts with Proteins of the Cytoskeleton in S. rosetta

Profiling of *S. rosetta* cell lysates yielded several hits assigned to membrane proteins (e.g. ATP-binding transporters) as well as proteins involved in the cytoskeleton formation (e.g. tubulin, cofilin, fascin and actin). These findings were intriguing as they suggested that IOR-1A might modulate or prevent the restructuring of the cellular organization, such as multicellular rosette formation, but without showing typical cytotoxicity effects as other microbial metabolites interacting with proteins of the cytoskeleton. We also questioned if IOR-1A interacts with enzymes involved in sphingolipid metabolism and signaling pathways of *S. rosetta.* While none of the in silico detected homologs were identified from on-bead digestion analysis, data sets obtained from in-gel digestion approaches contained protein hits assigned to homologs of eukaryotic serine palmitoyltransferases (SPTs, three homologs), as well as KDSRs (four

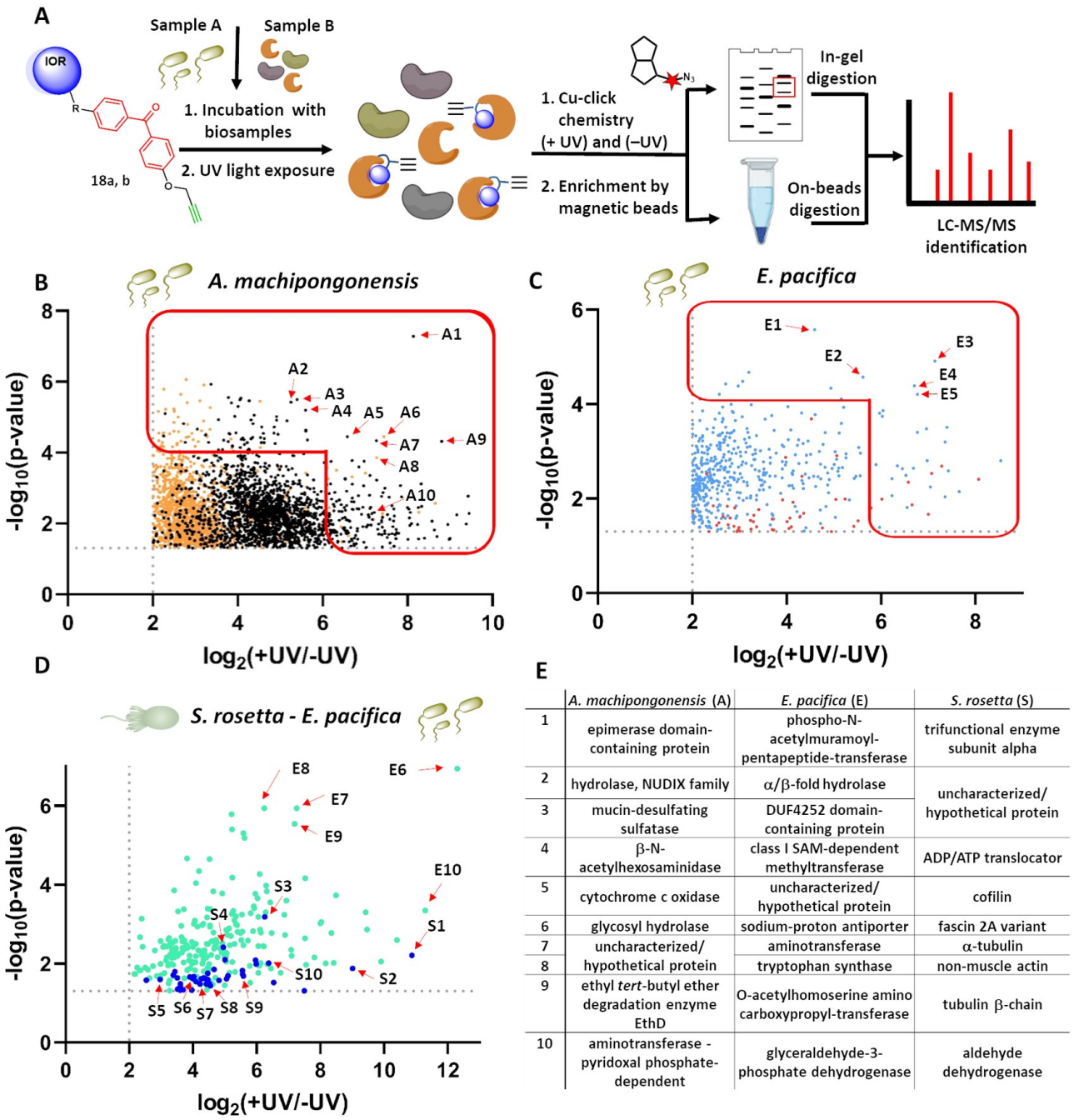

E

	A. machipongonensis (A)	*E. pacifica* (E)	*S. rosetta* (S)
1	epimerase domain-containing protein	phospho-N-acetylmuramoyl-pentapeptide-transferase	trifunctional enzyme subunit alpha
2	hydrolase, NUDIX family	α/β-fold hydrolase	uncharacterized/ hypothetical protein
3	mucin-desulfating sulfatase	DUF4252 domain-containing protein	
4	β-N-acetylhexosaminidase	class I SAM-dependent methyltransferase	ADP/ATP translocator
5	cytochrome c oxidase	uncharacterized/ hypothetical protein	cofilin
6	glycosyl hydrolase	sodium-proton antiporter	fascin 2A variant
7	uncharacterized/ hypothetical protein	aminotransferase	α-tubulin
8		tryptophan synthase	non-muscle actin
9	ethyl *tert*-butyl ether degradation enzyme EthD	O-acetylhomoserine amino carboxypropyl-transferase	tubulin β-chain
10	aminotransferase - pyridoxal phosphate-dependent	glyceraldehyde-3-phosphate dehydrogenase	aldehyde dehydrogenase

Figure 4. A) Scheme of the applied photo-affinity labelling-based analysis strategy using either living cells (sample A) or protein extracts from lysed bacterial cells (sample B). Cu-click chemistry was performed on previously irradiated (+UV) and non-irradiated (−UV) samples, which were then tagged and analyzed either after in-gel or on-bead digestion by nano-LC-ESI-MS/MS analysis. Volcano-plot visualization of protein abundance changes (threshold of $\log_2(+UV/-UV) > 2$ and p-value < 0.05) obtained using a label-free quantification protocol with samples obtained from B) *A. machipongonensis* PR1 (orange: treatment of intact cells; black: treatment of enriched proteins of cell lysates); C) *E. pacifica* KMM 6172 (light blue: treatment of intact cells; red: treatment of enriched proteins of cell lysates), the threshold for GO-assisted analysis of photo-crosslinked sequences (+UV) was set to a threshold of $\log_2(+UV/-UV) > 6$ with a p-value < 0.0001 (red box) and D) *S. rosetta* with co-cultured *E. pacifica* KMM 6172 (enriched proteins from mixed cell lysates, blue: *S. rosetta*; green: *E. pacifica* KMM 6172); E) Most significant hits and their putative annotations.

homologs), S1P lyases (one homolog), and ceramidases (two homologs), which indicated that bacterially produced IOR-1A could interact with sphingolipid-related pathways in *S. rosetta*.

Conclusion

In this study we elaborated on the function of the bacterial signaling molecule IOR-1A within the predator-prey rela-

tion of the rosette-forming choanoflagellate *S. rosetta* and co-occurring bacteria. With the aim to determine concentrations and possible proteogenic binding partners of the rosette-inhibitor IOR-1A, a new and scalable total synthesis of IOR-1A (27 % overall yield) and congeners has been developed. The modular synthetic approach requires only a total of six steps and makes use of a decarboxylative cross-coupling reaction of a tartaric acid derivative carrying a protected sulfonic acid moiety with alkyl zinc reagents of choice, which allows for late stage-modification.

The quantification of IOR-1A in nine rosette-inducing and two non-inducing bacterial strains demonstrated that IOR-1A was only present in cell membranes of a subset of bacterial strains that produced RIFs and induced rosette-formation, which let us to hypothesize that the biosynthesis of inducing RIFs and inhibitor IOR-1A are likely interlinked.

As fluorescently-labeled IOR-1A derivatives were taken up by *S. rosetta* and had inhibitory activity similar to the parent molecule in cellular assays, we employed probes for de novo chemical proteomic identification of IOR-1A-binding proteins. A first proof-of-concept study using probe **18a** allowed profiling potential binding partners in two sulfonosphingolipid-producing bacterial strains, *A. machipongonensis* and *E. pacifica*, as well as the choanoflagellate *S. rosetta.*

Evaluation of datasets resulted for the first time in the identification and prioritization of significant potential binding partners, which included enzyme hits related to biosynthesis and transport (e.g. homologs of sulfatases, hydrolases and aminotransferases) as well as cellular motility, rotational mechanisms and cellular structure of *S. rosetta*, which demonstrated the utility of the developed synthetic probes. With these results in hand, we are now spearheading the design of improved IOR probes specific for a single enzyme class to determine which interactions might relate to its rosette inhibitory activity and by that uncover the molecular mechanisms of rosette formation. The herein presented synthetic probes and methodology also open new possibilities to profile diverse bacterial strains, communities and choanoflagellates to elucidate the abundance and diversity of sphingolipid binding partners, also in more complex communities.

In summary, a new and modular synthetic approach to the bacterial sulfonolipid IOR-1A and chemical probes thereof was developed, which allowed elaborating on the biochemical foundations of rosette-formation in the choanoflagellate *S. rosetta.*

Experimental Section

The datasets supporting this article have been uploaded as ESI and contains details for chemical procedures, 1D and 2D NMR of described compounds, as well as HRMS data and bioassay data. This material is available free of charge.

Acknowledgements

We are grateful for financial support from the German Research Foundation (DFG, BE 4799/2-1). CB greatly acknowledges funding from the European Union's Horizon 2020 research and innovation program (ERC Grant number: 802736, MORPHEUS) and FUNR and NK thank the Howard Hughes Medical Institute. The work was also funded by the DFG Collaborative Research Center/Transregio FungiNet 124 (project Z2; project number 210879364) to OK. We would also like to thank Heike Heinecke (HKI) for recording NMR spectra. Open Access funding enabled and organized by Projekt DEAL.

Conflict of Interest

The authors declare no conflict of interest.

Data Availability Statement

The data that support the findings of this study are available in the Supporting Information of this article.

Keywords: Chemical Probes · Microbial Natural Products · Proteomic Profiling · Sphingolipids · Total Synthesis

[1] "3.04—Chemical Ecology of Choanoflagellates": J. P. Gerdt in *Comprehensive Natural Products III* (Eds.: H.-W. (Ben) Liu, T. P. Begley), Elsevier, Oxford, **2020**, pp. 45–65.
[2] A. Woznica, N. King, *Curr. Opin. Microbiol.* **2018**, *43*, 108–116.
[3] M. Roper, M. J. Dayel, R. E. Pepper, M. A. R. Koehl, *Phys. Rev. Lett.* **2013**, *110*, 228104.
[4] R. A. Alegado, L. W. Brown, S. Cao, R. K. Dermenjian, R. Zuzow, S. R. Fairclough, J. Clardy, N. King, *eLife* **2012**, *1*, e00013.
[5] D. Leichnitz, L. Raguž, C. Beemelmanns, *Chem. Soc. Rev.* **2017**, *46*, 6330–6344.
[6] S. T. Pruett, A. Bushnev, K. Hagedorn, M. Adiga, C. A. Haynes, M. C. Sullards, D. C. Liotta, A. H. J. Merrill, *J. Lipid Res.* **2008**, *49*, 1621–1639.
[7] D. Leichnitz, C.-C. Peng, L. Raguž, F. Rutaganira, T. Jautzus, L. Regestein, N. King, C. Beemelmanns, *Chem. Eur. J.* **2022**, *28*, e202103883.
[8] C. Beemelmanns, A. Woznica, R. A. Alegado, A. M. Cantley, N. King, J. Clardy, *J. Am. Chem. Soc.* **2014**, *136*, 10210–10213.
[9] A. Woznica, A. M. Cantley, C. Beemelmanns, E. Freinkman, J. Clardy, N. King, *Proc. Natl. Acad. Sci. USA* **2016**, *113*, 7894–7899.
[10] A. M. Cantley, A. Woznica, C. Beemelmanns, N. King, J. Clardy, *J. Am. Chem. Soc.* **2016**, *138*, 4326–4329.
[11] E. V. Ireland, A. Woznica, N. King, *Appl. Environ. Microbiol.* **2020**, *86*, e02920-19.
[12] P. J. Harrison, T. M. Dunnb, D. J. Campopiano, *Nat. Prod. Rep.* **2018**, *35*, 921–954.
[13] Y. A. Hannun, L. M. Obeid, *Nat. Rev. Mol. Cell Biol.* **2018**, *19*, 175–191.
[14] "Bacterial Sphingolipids and Sulfonolipids": O. Geiger, J. Padilla-Gómez, I. M. López-Lara in *Biogenesis of Fatty Acids, Lipids and Membranes. Handbook of Hydrocarbon and Lipid Microbiology* (Eds.: O. Geiger), Springer, Cham, **2019**.

[15] A. M. Cantley, J. Clardy, *Nat. Prod. Rep.* **2015**, *32*, 888–892.
[16] O. Geiger, N. González-Silva, I. M. López-Lara, C. Sohlenkamp, *Prog. Lipid Res.* **2010**, *49*, 46–60.
[17] J. B. Parsons, C. O. Rock, *Prog. Lipid Res.* **2013**, *52*, 249–276.
[18] E. L. Johnson, S. L. Heaver, J. L. Waters, B. I. Kim, A. Bretin A L Goodman, A. T. Gewirtz, T. S. Worgall, R. E. Ley, *Nat. Commun.* **2020**, *11*, 2471.
[19] J. Gubbens, E. Ruijter, L. E. V. de Fays, J. M. A. Damen, B. de Kruijff, M. Slijper, D. T. S. Rijkers, R. M. J. Liskamp, A. I. P. M. de Kroon, *Chem. Biol.* **2009**, *16*, 3–14.
[20] D. P. Murale, S. C. Hong, M. M. Haque, J. S. Lee, *Proteome Sci.* **2016**, *15*, 1–34.
[21] M. Soethoudt, S. C. Stolze, M. V. Westphal, L. van Stralen, A. Martella, E. J. van Rooden, W. Guba, Z. V. Varga, H. Deng, S. I. van Kasteren, U. Grether, A. P. Ijzerman, P. Pacher, E. M. Carreira, H. S. Overkleeft, A. Ioan-Facsinay, L. H. Heitman, M. van der Stelt, *J. Am. Chem. Soc.* **2018**, *140*, 6067–6075.
[22] L. Raguž, C.-C. Peng, M. Kaiser, H. Görls, C. Beemelmanns, *Angew. Chem. Int. Ed.* **2022**, *61*, e202112616; *Angew. Chem.* **2022**, *134*, e202112616.
[23] J. Cornella, J. T. Edwards, T. Qin, S. Kawamura, J. Wang, C.-M. Pan, R. Gianatassio, M. Schmidt, M. D. Eastgate, P. S. Baran, *J. Am. Chem. Soc.* **2016**, *138*, 2174–2177.
[24] T. Qin, J. Cornella, C. Li, L. R. Malins, J. T. Edwards, S. Kawamura, B. D. Maxwell, M. D. Eastgate, P. S. Baran, *Science* **2016**, *352*, 801–805.
[25] J. T. Edwards, R. R. Merchant, K. S. McClymont, K. W. Knouse, T. Qin, L. R. Malins, B. Vokits, S. A. Shaw, D. H. Bao, F. L. Wei, T. Zhou, M. D. Eastgate, P. S. Baran, *Nature* **2017**, *545*, 213–218.
[26] J. N. deGruyter, L. R. Malins, L. Wimmer, K. J. Clay, J. Lopez-Ogalla, T. Qin, J. Cornella, Z. Liu, G. Che, D. Bao, J. M. Stevens, J. X. Qiao, M. P. Allen, M. A. Poss, P. S. Baran, *Org. Lett.* **2017**, *19*, 6196–6199.
[27] J. R. Walker, C. D. Poulter, *J. Org. Chem.* **2005**, *70*, 9955–9959.
[28] E. A. Mash, K. A. Nelson, S. Van Deusen, S. B. Hemperly, *Org. Synth.* **1990**, *68*, 92.
[29] A. M. Ali, B. Hill, S. D. Taylor, *J. Org. Chem.* **2009**, *74*, 3583–3586.
[30] S. C. Miller, *J. Org. Chem.* **2010**, *75*, 4632–4635.
[31] D. H. R. Barton, A. Gateauolesker, S. D. Gero, B. Lacher, C. Tachdjian, S. Z. Zard, *J. Chem. Soc. Chem. Commun.* **1987**, 1790–1792.
[32] D. H. R. Barton, A. Gateauolesker, S. D. Gero, B. Lacher, C. Tachdjian, S. Z. Zard, *Tetrahedron* **1993**, *49*, 4589–4602.
[33] K. Masuda, M. Nagatomo, M. Inoue, *Nat. Chem.* **2017**, *9*, 207–212.
[34] W. M. Pearlman, *Tetrahedron Lett.* **1967**, *8*, 1663–1664.
[35] E. J. Alexy, H. Zhang, B. M. Stoltz, *J. Am. Chem. Soc.* **2018**, *140*, 10109–10112.
[36] A. E. Strom, J. F. Hartwig, *J. Org. Chem.* **2013**, *78*, 8909–8914.
[37] S. F. Kotarski, A. A. Salyers, *J. Bacteriol.* **1984**, *158*, 102–109.
[38] M. J. Dayel, R. A. Alegado, S. R. Fairclough, T. C. Levin, S. A. Nichols, K. McDonald, N. King, *Dev. Biol.* **2011**, *357*, 73–82.
[39] T. T. Hoffmeyer, P. Burkhardt, *Curr. Opin. Genet. Dev.* **2016**, *39*, 42–47.
[40] D. Laundon, B. T. Larson, K. McDonald, N. King, P. Burkhardt, *PLoS Biol.* **2019**, *17*, e30002266.
[41] R. T. Riley, A. H. Merrill, Jr., *J. Lipid Res.* **2019**, *60*, 1183–1189.
[42] M. Á. Vences-Guzmán, R. Peña-Miller, N. A. Hidalgo-Aguilar, M. L. Vences-Guzmán, Z. Guan, C. Sohlenkamp, *Environ. Microbiol.* **2021**, *23*, 2448–2460.
[43] L. Hou, H. Y. Tian, L. Wang, Z. E. Ferris, J. Wang, M. Cai, E. A. Older, M. R. K. Raja, D. Xue, W. Sun, P. Nagarkatti, M. Nagarkatti, H. Chen, D. Fan, X. Tang, J. Li, *ACS Chem. Biol.* **2022**, *17*, 1197–1206.
[44] M. H. Wright, S. A. Sieber, *Nat. Prod. Rep.* **2016**, *33*, 681–708.
[45] R. Pattipeiluhu, S. Crielaard, I. Klein-Schiphorst, B. I. Florea, A. Kros, F. Campbell, *ACS Cent. Sci.* **2020**, *6*, 535–545.
[46] X. Chen, Y. K. Wong, J. Wang, J. Zhang, Y. M. Lee, H. M. Shen, Q. Lin, Z. C. Hua, *Proteomics* **2017**, *17*, 3–4.
[47] P. Haberkant, F. Stein, D. Höglinger, M. J. Gerl, B. Brügger, P. P. Van Veldhoven, J. Krijgsveld, A.-C. Gavin, C. Schultz, *ACS Chem. Biol.* **2016**, *11*, 222–230.
[48] a) Data deposited to the ProteomeXchange Consortium via the PRIDE partner repository with the dataset identifier PXD034064; b) Y. Perez-Riverol, J. Bai, C. Bandla, S. Hewapathirana, D. García-Seisdedos, S. Kamatchinathan, D. Kundu, A. Prakash, A. Frericks-Zipper, M. Eisenacher, M. Walzer, S. Wang, A. Brazma, J. A. Vizcaíno, *Nucleic Acids Res.* **2022**, *50*, D543–D552.
[49] G. Bindea, B. Mlecnik, H. Hackl, P. Charoentong, M. Tosolini, A. Kirilovsky, W. H. Fridman, F. Pagès, Z. Trajanoski, J. Galon, *Bioinformatics* **2009**, *25*, 1091–1093.
[50] H. C. Beck, *FEMS Microbiol. Lett.* **2005**, *243*, 37–44.
[51] F. Parveen, D. Bender, S.-H. Law, V. K. Mishra, C.-C. Chen, L. Y. Ke, *Cell* **2019**, *8*, 1573.
[52] G. Stankeviciute, P. Tang, B. Ashley, J. D. Chamberlain, M. E. B. Hansen, A. Coleman, R. D'Emilia, L. Fu, E. C. Mohan, H. Nguyen, Z. Guan, D. J. Campopiano, E. A. Klein, *Nat. Chem. Biol.* **2022**, *18*, 305–312.
[53] A. Woznica, J. P. Gerdt, R. E. Hulett, J. Clardy, N. King, *Cell* **2017**, *170*, 1175–1183, e11.
[54] T. F. Braun, M. J. McBride, *J. Bacteriol.* **2005**, *187*, 2628–37.
[55] R. H. White, *J. Bacteriol.* **1984**, *159*, 42–46.

Manuscript received: June 21, 2022
Accepted manuscript online: July 28, 2022
Version of record online: September 5, 2022